










RESEARCH ARTICLE | AUGUST 21 2024

## MeV proton and neutron damage effects on deep-ultraviolet light-emitting diodes

Special Collection: [Celebrating the Achievements and Life of Paul H. Holloway](#)

Jian-Sian Li ; Chao-Ching Chiang ; Hsiao-Hsuan Wan ; Jihyun Kim ; Simon Barke ; Peter Wass ; Fan Ren ; John W. Conklin ; S. J. Pearton 



*J. Vac. Sci. Technol. B* 42, 052206 (2024)

<https://doi.org/10.1116/6.0003818>



**HIDEN**  
ANALYTICAL

## Instruments for Advanced Science

- Knowledge
- Experience ■ Expertise

[Click to view our product catalogue](#)

Contact Hiden Analytical for further details:

[www.HidenAnalytical.com](http://www.HidenAnalytical.com)  
[info@hiden.co.uk](mailto:info@hiden.co.uk)

### Gas Analysis



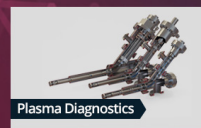
- ▶ dynamic measurement of reaction gas streams
- ▶ catalysis and thermal analysis
- ▶ molecular beam studies
- ▶ dissolved species probes
- ▶ fermentation, environmental and ecological studies

### Surface Science



- ▶ UHV TPD
- ▶ SIMS
- ▶ end point detection in ion beam etch
- ▶ elemental imaging - surface mapping

### Plasma Diagnostics



- ▶ plasma source characterization
- ▶ etch and deposition process reaction kinetic studies
- ▶ analysis of neutral and radical species

### Vacuum Analysis



- ▶ partial pressure measurement and control of process gases
- ▶ reactive sputter process control
- ▶ vacuum diagnostics
- ▶ vacuum coating process monitoring

# MeV proton and neutron damage effects on deep-ultraviolet light-emitting diodes

Cite as: J. Vac. Sci. Technol. B 42, 052206 (2024); doi: 10.1116/6.0003818

Submitted: 11 June 2024 · Accepted: 24 July 2024 ·

Published Online: 21 August 2024



Jian-Sian Li,<sup>1,a)</sup> Chao-Ching Chiang,<sup>1</sup> Hsiao-Hsuan Wan,<sup>1</sup> Jihyun Kim,<sup>2</sup> Simon Barke,<sup>3</sup> Peter Wass,<sup>3</sup> Fan Ren,<sup>1</sup> John W. Conklin,<sup>3</sup> and S. J. Pearton<sup>3</sup>

## AFFILIATIONS

<sup>1</sup>Department of Chemical Engineering, University of Florida, Gainesville, Florida 32611

<sup>2</sup>Department of Chemical and Biological Engineering, Seoul National University, Seoul 08826, Republic of Korea

<sup>3</sup>Department of Mechanical and Aerospace Engineering, University of Florida, Gainesville, Florida 32611

<sup>4</sup>Department of Materials Science and Engineering, University of Florida, Gainesville, Florida 32611

**Note:** This paper is part of the Special Topic Collection Celebrating the Achievements and Life of Paul H. Holloway.

**a)Electronic mail:** [jjansianli@uf.edu](mailto:jjansianli@uf.edu)

## ABSTRACT

270 nm deep-ultraviolet AlGaIn light-emitting diodes were irradiated with either neutrons or 15 MeV protons. Neutrons produced via charge-exchange reactions of <sup>9</sup>Be with protons exhibited energy ranges from 0 to 33 MeV, with an average energy of approximately 9.8 MeV. The fluences ranged from  $1.1 \times 10^{14}$  to  $2.2 \times 10^{14}$  neutrons cm<sup>-2</sup> and  $10^{13}$  or  $10^{14}$  protons cm<sup>-2</sup>. Two primary degradation modes were observed: increased trap-assisted tunneling, indicated by an initial reduction in turn-on voltage, and a decrease in carrier concentration, shown by reduced forward current due to deep state formation. For instance, 15 MeV proton irradiation resulted in more than an order of magnitude reduction in reverse current at a fluence of  $10^{14}$  ions cm<sup>-2</sup>. The decrease in subthreshold leakage current at higher fluences of neutrons and protons is attributed to defect-induced carrier trapping, thereby reducing layer conductivity across the p-n junction. Emission intensity decreased with fluence for both protons and neutrons, without a measurable increase in midgap emission. The nonlinear degradation in current and light output with fluence suggests strong dynamic recombination of defects during irradiation of high aluminum alloys.

Published under an exclusive license by the AVS. <https://doi.org/10.1116/6.0003818>

## I. INTRODUCTION

Deep-ultraviolet light-emitting diodes (UVC LEDs) are used in many applications, including sterilization, water purification, and medical diagnostics.<sup>1–5</sup> These LEDs emit light in the deep-ultraviolet wavelength range (230–300 nm) and are effective in deactivating various microorganisms due to the strong absorption in this emission range by DNA and RNA.<sup>3–6</sup> In general, the external quantum efficiency (EQE) is very low, <0.5% in Al<sub>x</sub>Ga<sub>1-x</sub>N-based deep-UVC (200–280 nm) LEDs. However, values of EQE >10% have been reported in optimized device structures.<sup>6–15</sup>

In contrast to the more common UV sources such as Hg lamps and excimer lasers,<sup>1–15</sup> UVC LEDs have advantages such as compactness, longer lifetimes, and the capability for modulation at higher frequencies. Furthermore, their potential utilization in the future space mission Laser Interferometer Space Antenna (LISA) for discharge capability on free-flying test masses to mitigate

electrostatic force effects induced by cosmic rays and solar particles is documented,<sup>16–20</sup> along with the required reliability for long space missions.<sup>21–23</sup> In addition, in the new GRATTIS mission, the technology used is very similar to the LISA gravity reference sensors but designed for tracking climate change and global warming effects on Earth.<sup>24</sup>

However, comprehending the response of the high Al-content AlGaIn layers within the LEDs to diverse radiation environments, under total ionizing dose (TID) conditions dominated by ionization energy deposition and during single event upsets triggered by heavy ion strikes, remains a significant area of investigation.<sup>18,21,25–34</sup> Saraf *et al.*<sup>19</sup> conducted experiments on UVC LEDs, irradiating them with ~63 MeV protons up to fluences of  $2 \times 10^{12}$  protons cm<sup>-2</sup>, simulating a radiation dose equivalent to approximately 100 years in the LISA orbit. They observed negligible changes in light output. The resistance to radiation-induced displacement effects is attributed to strong atomic bonding and high defect recombination rates

04 September 2024 19:12:10

at room temperature in high aluminum content alloys, highlighting their suitability for space and extreme terrestrial environments. Their response to radiation sources such as gamma rays,<sup>25</sup> neutrons, and electrons<sup>30</sup> necessitates further study. The atmospheric neutron energy spectrum at sea level ranges from  $10^{-9}$  to  $10^3$  MeV and neutron fluence per lethargy ranges up to  $14 \times 10^{-4}$   $\text{cm}^2 \text{ s}^{-1}$ , where lethargy is a measure of neutron slowing, calculated as the logarithm of a reference energy  $E_0$  to the current energy  $E$ .<sup>35–37</sup> At sea level in New York City, the peak neutron flux exhibits a distribution characterized by approximately four thermal neutrons per square centimeter per hour ( $\text{n cm}^{-2} \text{ h}^{-1}$ ) with an energy of around 0.025 eV, roughly 13 high-energy neutrons ( $\text{n cm}^{-2} \text{ h}^{-1}$ ) with an energy of 10 MeV and around 20 mid-range energy neutrons ( $\text{n cm}^{-2} \text{ h}^{-1}$ ) with an energy of 1 MeV.<sup>36,37</sup> The spectral fluence, denoted by  $\phi(E)$  with units of neutrons per square centimeter per mega electron volt ( $\text{n cm}^{-2} \text{ MeV}^{-1}$ ), quantifies the energy deposited per unit volume ( $\text{cm}^3$ ) through atomic displacements caused by neutrons.<sup>36,37</sup> In instances where fast neutrons induce significant recoil cascades, carrier removal transpires within disordered regions where the core's Fermi level becomes pinned.<sup>27</sup>

Radiation-induced damage in LEDs can lead to lower emission intensity, lower leakage current and breakdown voltage, and the generation of defects such as vacancies and interstitials capable of trapping carriers and facilitating nonradiative recombination.<sup>21,31–38</sup> Notably, Wang *et al.*<sup>25</sup> reported that  $\gamma$ -ray irradiation accelerated the subsequent degradation under normal operation, with the degradation being inversely proportional to the cube of the LED current.

This study presents the response of UVC LEDs to MeV neutrons and protons. We find a similar response of the LEDs to both types of radiation. Even at fluences up to  $10^{14}$   $\text{cm}^{-2}$ , there was no new midgap emission induced. Similarly, there was less than a factor of ten decrease in band-edge emission. The degradation mechanisms in the LEDs are related to more trap-assisted tunneling and loss of carriers to trapping in radiation-induced defect states.

## II. EXPERIMENT

The packaged LEDs (Klaran LA Series) had peak emission in the range of 260–270 nm. The total output power was  $>80$  mW and the LEDs were manufactured by Crystal IS. These LEDs were mounted in  $3.5 \times 3.5$   $\text{mm}^2$  surface mount diode packages. The epitaxial layers were grown by metal organic chemical vapor deposition on a c-plane (0001) AlN single crystal substrate. The epitaxial structure was initiated with a buffer layer  $\sim 1 \mu\text{m}$  thick, composed of Si-doped  $\text{Al}_{0.76}\text{Ga}_{0.24}\text{N}$ , followed by a 100 nm transition layer of Si-doped  $\text{Al}_{0.65}\text{Ga}_{0.35}\text{N}$  and succeeded by a multiquantum well configuration comprising alternating pairs of  $\text{Al}_{0.58}\text{Ga}_{0.42}\text{N}$  wells and  $\text{Al}_{0.7}\text{Ga}_{0.3}\text{N}$  barriers. An electron blocking layer preceded the p-GaN top contact layer. Additional details regarding the growth and fabrication of LEDs have been provided previously.<sup>38</sup>

The experiment employed neutron irradiation conducted at the Korea Institute of Radiological and Medical Science (KIRAMS). A 45 MeV MC-50 cyclotron served as the neutron source. Nuclear reactions induced by 35 MeV protons colliding with beryllium (Be) targets generated the neutron flux. Prior to interacting with the Be target, the proton beam passed through two aluminum (Al) degrader foils to achieve the desired final energy (35 MeV). The

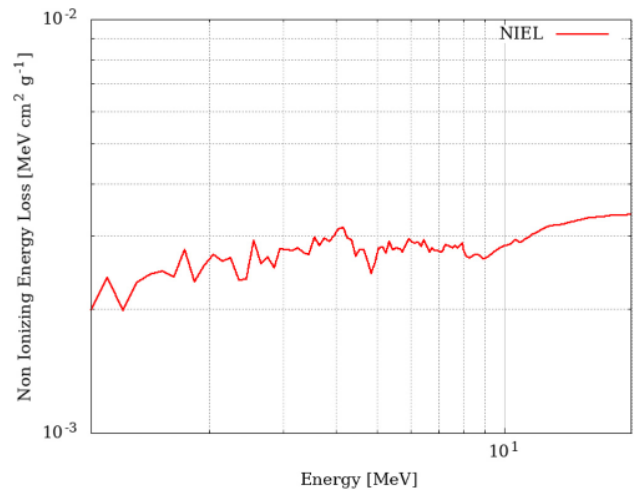


**FIG. 1.** Non-ionizing Energy Loss (NIEL) calculation for neutrons in AlN, assuming displacement threshold energies of 50 and 20 eV, respectively, for Al and N and a fluence of  $10^{14}$   $\text{cm}^{-2}$ .

main mechanism for creating neutrons involved charge-exchange reactions of  ${}^9\text{Be}$  ( $p; n$ )  ${}^9\text{Be}$ , with a proton-to-neutron generation ratio of 8200:1. The average energy of the neutrons was  $\sim 9.8$  MeV. The devices underwent irradiation for 2 or 4 h, with a total fluence of either  $1.1 \times 10^{14}$  or  $2.2 \times 10^{14}$  neutrons  $\text{cm}^{-2}$ . The LEDs were not biased during the neutron irradiation process. Figure 1 shows the nonionizing energy loss created by neutrons in AlN as a function of energy.<sup>39,40</sup> As will be seen later, this is approximately a factor of five lower than for the protons and represents the energy lost to creating lattice displacements.

The same cyclotron was utilized for proton irradiation of the LEDs. Samples were irradiated from the back of their packages, without applying any external bias voltage. The proton beam energy was held constant at 15 MeV. The irradiation fluence was varied between  $10^{13}$  and  $10^{14}$  protons per square centimeter ( $\text{cm}^2$ ) at a constant beam current of 10 nanoamperes (nA). For comparison, the proton fluence an LED would receive in one year within the LISA orbit is estimated to be approximately  $2 \times 10^{10}$   $\text{cm}^{-2}$ .

The STOPPING AND RANGE OF IONS IN MATTER (SRIM) software<sup>41</sup> was employed to estimate the projected range of protons within the LEDs. Simulations indicated a range of approximately 600 micrometers ( $\mu\text{m}$ ) (Fig. 2), suggesting that protons penetrate the entire conductive substrate and potentially induce damage throughout all LED layers.

Furthermore, the SR-NIEL simulator<sup>39,40</sup> was used to assess the distribution of vacancy density within the material as a function of the proton irradiation energy. As shown in Fig. 3, the nonionizing energy loss at 15 MeV was determined to be  $\sim 10^{-2}$   $\text{MeV cm}^2 \text{ g}^{-1}$ . While this value is non-negligible, it is important to note that this energy loss is primarily dissipated as heat and does not contribute directly to lattice damage in the material.

The linear energy transfer (LET), which quantifies the average energy deposited by protons per unit track length, indicated that

04 September 2024 19:12:10

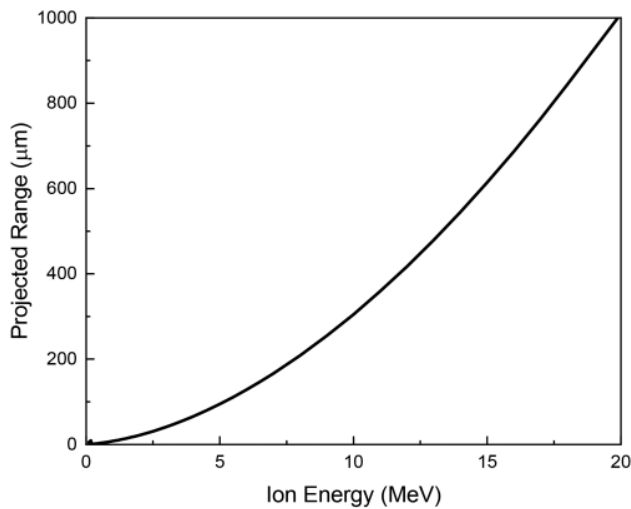


FIG. 2. Projected range of protons obtained from SRIM.

the Bragg peak (region of maximum energy deposition) lies beyond the surface of the LED structure. Additionally, the LET value remained relatively constant throughout the LED due to the chosen proton energy.

The electrical properties of the LEDs were investigated using current-voltage ( $I$ - $V$ ) characteristics obtained with an Agilent 4156C parameter analyzer. An Avantes AvaSpec-ULS2048XL-EVO spectrometer equipped with fiber-optic coupling facilitated the recording of emission spectra. A 600  $\mu\text{m}$  diameter fiber optic cable

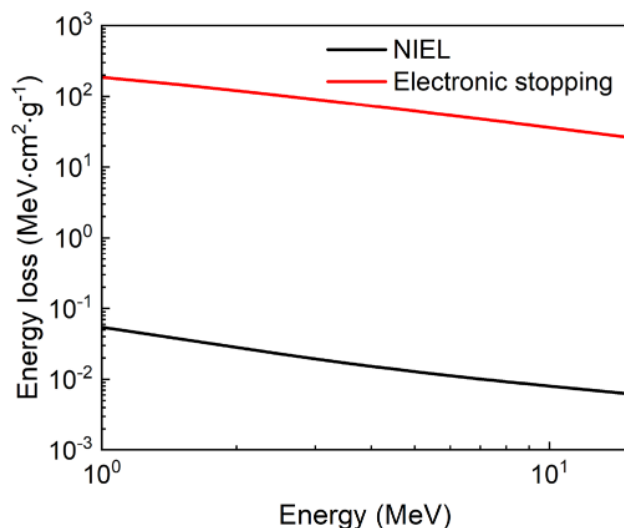


FIG. 3. Electronic and nonionizing energy loss for protons in AlN.

served as the coupling element between the spectrometer and the ultraviolet (UV) LEDs.

For approximate total output power measurements, the LEDs were coupled to a silicon (Si) photodetector connected in series with a 55  $\Omega$  resistor. The voltage across the resistor was measured, and the resultant power was calculated. It is acknowledged that previous research has documented inherent statistical variations in spectral characteristics across large batches of LEDs.<sup>21–23</sup> Therefore, the primary application of the acquired intensity spectra lies in comparing the shape of the emission peak at different irradiation levels. To isolate the effects of irradiation and ensure conclusive results, the same LEDs were measured before and after undergoing irradiation.

### III. RESULTS AND DISCUSSION

Figure 4(a) shows the  $I$ - $V$  characteristic from the LEDs before and after neutron irradiation at the two fluences. The dominant effect is a reduction in both forward and reverse current, which must result from a reduction in the effective carrier concentration on both sides of the p-n junction.<sup>42–44</sup> Gallium vacancies are the predominant defects introduced in II-nitrides as a result of particle irradiation and introduce deep acceptor levels around 0.9–1.3 eV above the valence band, whereas in AlN, the vacancy levels are generally deeper, often reported near 1.8–2.4 eV above the valence band. These values can be influenced by factors such as strain, doping, and the presence of other defects. These deep acceptors will compensate the n-type doping in the LED structure.

For neutrons, lattice damage in the LEDs arises predominantly from scattering interactions within the energy spectrum up to 30 MeV.<sup>45</sup> The mean free path ( $\lambda$ ) for neutron scattering interactions was assessed using MONTE CARLO N-PARTICLE TRANSPORT CODE (MCNP) software,<sup>45</sup> exceeding 1 cm across the neutron energy spectrum to 30 MeV in AlN. This is larger than the AlN substrate thickness of approximately 600  $\mu\text{m}$ , indicating the neutrons create defects throughout the entire active region of the LED structure. A noteworthy observation is the correlation between lower fluence and a decrease in turn-on voltage within the forward current characteristics. This trend signifies the introduction of an additional trap-assisted tunneling component. The formation of generation-recombination centers during irradiation is the underlying mechanism. These centers act as traps for free carriers, consequently reducing their concentration within the active region layers of the device. This decline in carrier concentration persists even beyond the turn-on voltage, manifesting as a reduction in current observed in the linear region of the  $I$ - $V$  characteristics depicted in Fig. 4(b).

The rate of recombination via tunneling exhibits a proportional relationship with the induced trap density and the capture rates for both electrons and holes.<sup>42,46–51</sup> Furthermore, the current density is directly proportional to the carrier density according to the Poisson and drift-diffusion equations.<sup>43,45</sup> Therefore, a reduction in carrier density within the p-n junction inevitably leads to a decrease in both forward and reverse currents.

The emission intensity of the LEDs was also reduced by the neutron irradiation, as shown in Fig. 5(a). The decrease in intensity is not linear with fluence, which suggests the dynamic annealing or immediate annihilation of created defects may be occurring. AlN

04 September 2024 19:12:10

and related alloys are known to have high defect recombination rates during irradiation.<sup>52–54</sup> The reduced output power after irradiation is shown in Fig. 5(b). Note that these powers are reduced from their absolute values because they are measured at some distance (2 cm) from the devices. In addition, there is no measurable increase in midgap emission after irradiation, indicating the trap states created are nonradiative.

Figure 6(a) shows the  $I$ - $V$  characteristics before and after the proton irradiations. Similar overall trends are seen as with the neutron damage. These include the fact that the the initial decrease in turn-on voltage observed at lower fluence is attributed to the introduction of trap-assisted tunneling mechanisms. However, the

trend reverses with the highest fluence, leading to a significant reduction in both forward and reverse currents.

This contrasting behavior can be explained by considering the competing effects at different fluence levels. At lower fluence, trap-assisted tunneling dominates, effectively lowering the barrier for carrier injection and leading to a decrease in turn-on voltage. However, with increasing fluence, the dominant effect shifts towards a significant loss of free carriers due to trapping at the newly formed generation-recombination centers. This depletion of carriers ultimately reduces the overall conductivity, resulting in a substantial decrease in both forward and reverse currents. At higher doses, the trend reverses because of the greater loss of

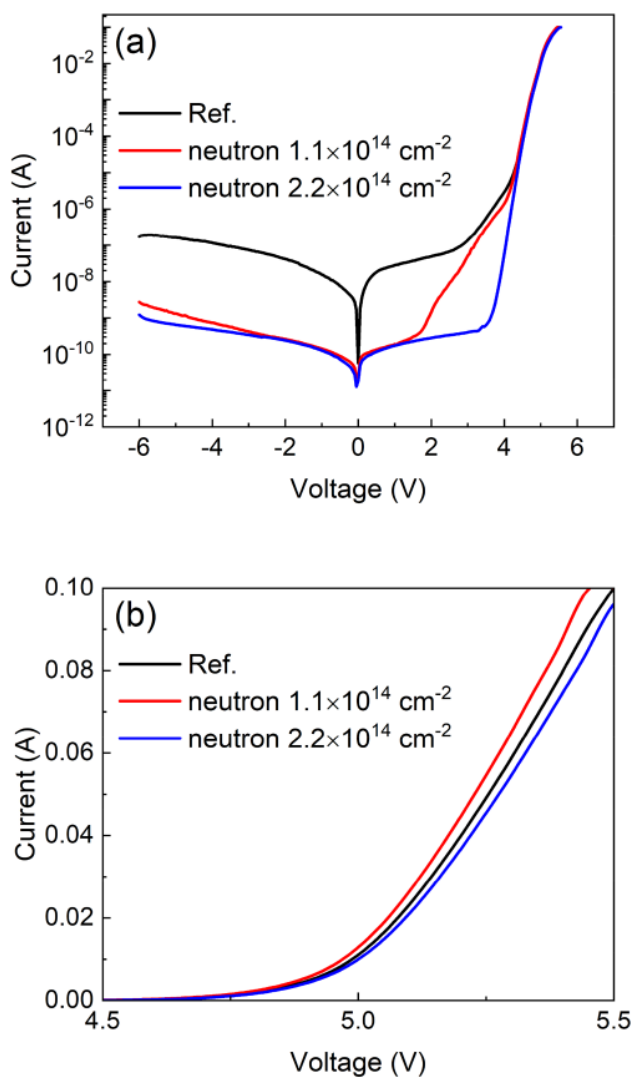


**FIG. 4.**  $I$ - $V$  characteristics from the UVC LEDs on (a) log or (b) linear scale before and after neutron irradiation.

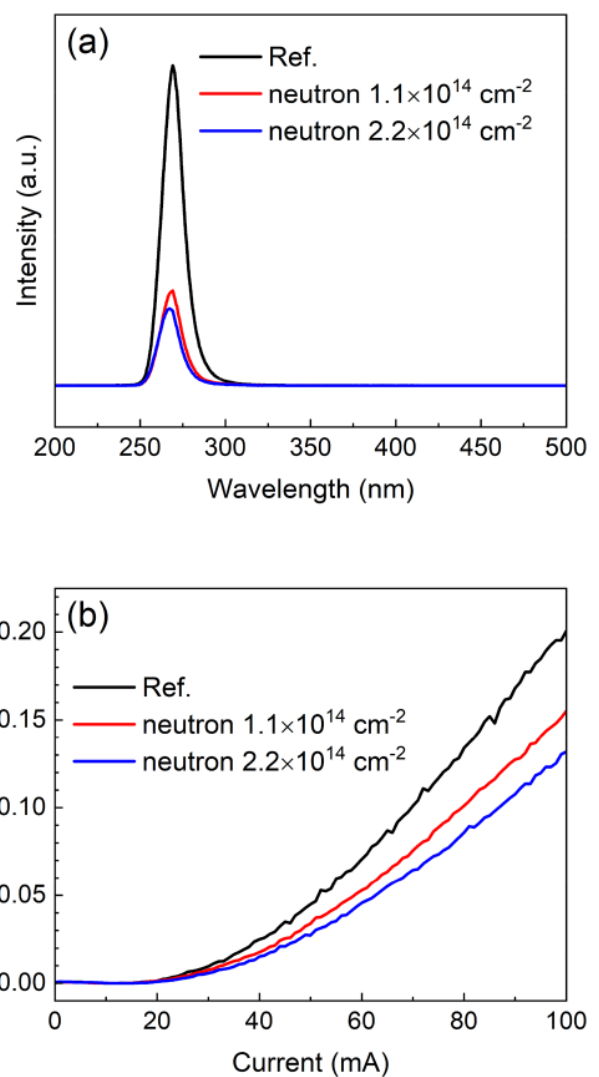


**FIG. 5.** Relative emission intensity of the UVC LEDs before and after neutron irradiation (a) and the relative integrated output power (b).

04 September 2024 19:12:10

carriers. The current beyond turn-on is also reduced by the irradiation Fig. 6(b), as seen for the neutrons.

The reduction in output emission intensity after the proton irradiations is shown in Fig. 7(a). There are several points of note. First, the higher fluence corresponds to  $\sim 10^4$  years in the LISA orbit<sup>18</sup> and  $4 \times 10^5$  years in low earth orbit, showing the ability of the UVC LEDs to withstand displacement damage effects in spaceborne applications. Second, the decreases are broadly similar to those created by the neutrons, even though the nonionizing energy loss per proton is higher. This reflects the difference in distribution of defects created, with isolated point defects in the case of protons and defect clusters in the case of neutrons.

The trap states created have not yet been established. Roccatto *et al.*<sup>45,46</sup> found states at  $E_C - 0.94$ , 3.06 and 3.5 eV were important in correlating an increase in trap-assisted tunneling of UVC LED during bias-aging experiments and that these were located near the electron blocking layer. Lee *et al.*<sup>29,30</sup> found in 436 nm LEDs that the decrease in the emission efficiency after irradiation with MeV electrons at fluences  $> 5 \times 10^{15} \text{ cm}^{-2}$  was correlated to the increase in concentration of  $E_C - 0.7 \text{ eV}$  electron traps in the active MQW region. This increase in trap density was accompanied by an increase in both diode series resistance and ideality factor. More work is needed to establish the specific traps states induced in UVC LEDs by both neutron and proton irradiation.

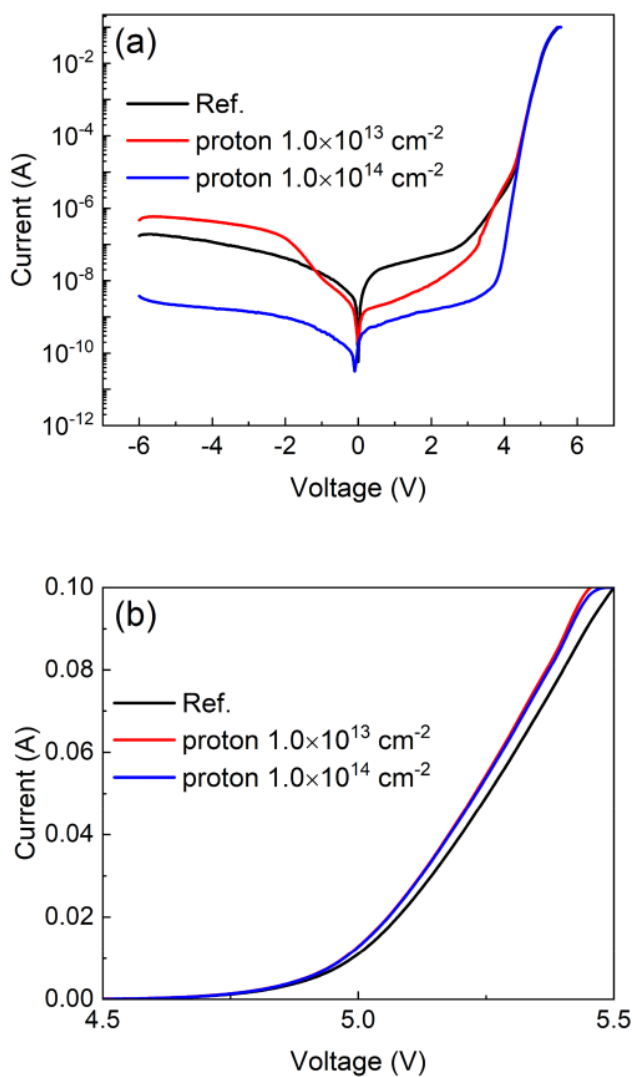


**FIG. 6.**  $I$ - $V$  characteristics of the UVC LEDs on (a) log or (b) linear scale before and after proton irradiation.

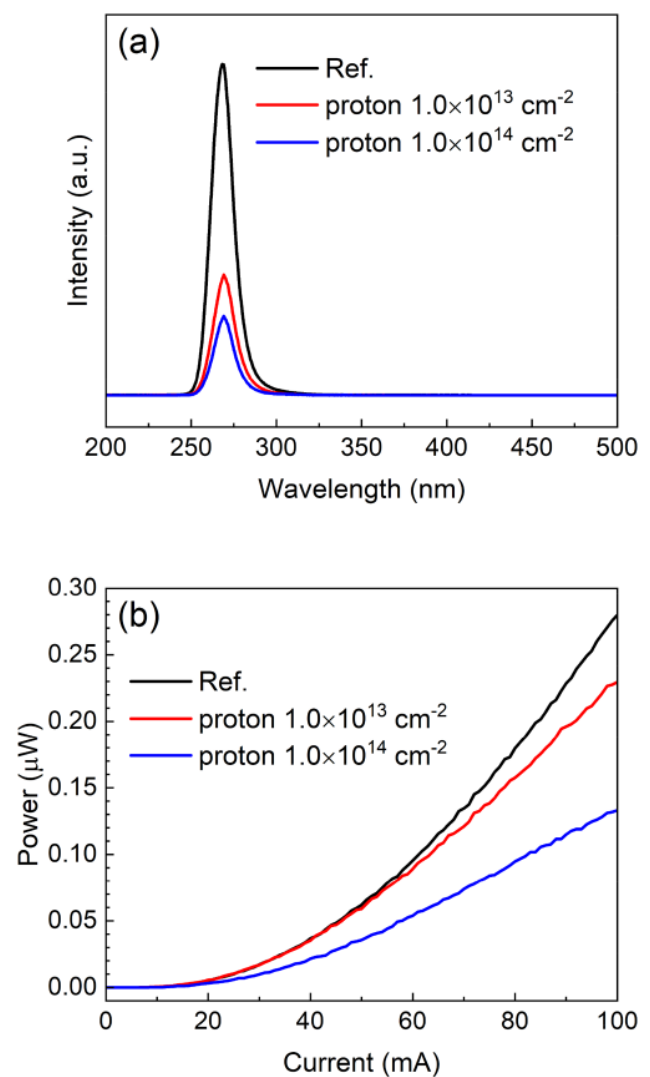


**FIG. 7.** Emission intensity of the UVC LEDs before and after proton irradiation (a) and the relative integrated output power (b).

04 September 2024 19:12:10

#### IV. SUMMARY AND CONCLUSIONS

In conjunction with geomagnetically trapped particles and galactic cosmic rays, solar protons and cosmic ray neutrons have the potential to present a threat to both manned spaceflight and the electronics and photonics utilized in space craft and satellite subsystems and instrumentation. Understanding the physical mechanisms underlying radiation-induced harm in UVC LEDs needs additional work, but our results show the capabilities of existing commercial UVC LEDs based on high-Al content AlGaN layers for survival in a variety of space-borne orbit applications, with unshielded radiation hardness to protons and neutrons more than two orders of magnitude greater than Si electronics. An elevation in subthreshold leakage current was observed across all irradiated devices, due to an increase in defects that increase trap-assisted tunneling and decrease the effective carrier density throughout the active region. The increase in leakage current below turn-on, resulting from irradiation, can be attributed to an increase in trap-assisted tunneling. The change in I-V characteristics indicate an increase in the density of deep-level traps within the inter-layer volume proximal to the electron blocking layer (EBL). These defects diminish the conductivity of the active layers in the LEDs. None of the irradiation conditions produced a significant increase in midgap emission.

#### ACKNOWLEDGMENTS

This work was supported by NASA Earth Science Technology Office (ESTO) Contract No. 80NSSC22K0288. The work at UF was also performed as part of Interaction of Ionizing Radiation with Matter University Research Alliance (IIRM-URA), sponsored by the Department of the Defense, Defense Threat Reduction Agency under Award No. HDTRA1-20-2-0002. The content of the information does not necessarily reflect the position or the policy of the federal government, and no official endorsement should be inferred. The work in Korea was supported by the Korea Institute for Advancement of Technology (KIAT) (No. P0012451, The Competency Development Program for Industry Specialist), the National Research Foundation of Korea (No. 2020M3H4A3081799) and the K-Sensor Development Program (No. RS-2022-00154729), funded by the Ministry of Trade, Industry and Energy (MOTIE, Korea), the Institute of Civil Military Technology Cooperation Center funded by the Defense Acquisition Program Administration and Ministry of Trade, Industry and Energy, and of Korean government (No. 20-CM-BR-05) and Korea Research Institute for defense Technology planning and advancement (KRIT) grant funded by Defense Acquisition Program Administration (DAPA) (Nos. KRIT-CT-21-034 and KRIT-CT-22-046).

#### AUTHOR DECLARATIONS

##### Conflict of Interest

The authors have no conflicts to disclose.

##### Author Contributions

**Jian-Sian Li:** Conceptualization (equal); Investigation (equal); Methodology (equal); Writing – original draft (equal); Writing –

review & editing (equal). **Chao-Ching Chiang:** Methodology (equal). **Hsiao-Hsuan Wan:** Methodology (equal). **Jihyun Kim:** Methodology (equal); Writing – review & editing (equal). **Simon Barke:** Methodology (equal); Writing – review & editing (equal). **Peter Wass:** Methodology (equal); Writing – review & editing (equal). **Fan Ren:** Methodology (equal); Writing – review & editing (equal). **John W. Conklin:** Methodology (equal); Writing – review & editing (equal). **S. J. Pearton:** Methodology (equal); Writing – original draft (equal); Writing – review & editing (equal).

#### DATA AVAILABILITY

The data that support the findings of this study are available within the article.

#### REFERENCES

- H. Hirayama, "Recent progress in AlGaN deep-UV LEDs," in *Light-Emitting Diodes*, edited by J. Thirumalai (IntechOpen, Rijeka, 2018), Chap. 7.
- M. S. Shur and R. Gaska, *IEEE Trans. Electron Devices* **57**, 12 (2010).
- N. Trivellini, D. Fiorimonte, F. Piva, M. Buffolo, C. De Santi, G. Meneghesso, E. Zanoni, and M. Meneghini, *Electronics* **11**, 728 (2022).
- W. Kowalski, *Ultraviolet Germicidal Irradiation Handbook* (Springer, Berlin, 2009).
- H. Inagaki, A. Saito, H. Sugiyama, T. Okabayashi, and S. S. Fujimoto, *Emerg. Microb. Infect.* **9**, 1744 (2020).
- H. Amano *et al.*, *J. Phys. D: Appl. Phys.* **53**, 503001 (2020).
- Michael Kneissl, T. Y. Seong, Jung Han, and Hiroshi Amano, *Nat. Photonics* **13**, 233 (2019).
- M. Guttman, M. Hermann, J. Enslin, S. Graupeter, L. Sulmoni, C. Kuhn, T. Wernicke, and M. Kneissl, "Improved light extraction and quantum efficiencies for UVB LEDs with UV-transparent p-AlGaN superlattices," *Proc. SPIE* **10104**, 101041S (2017).
- Takayoshi Takano, Takuya Mino, Jun Sakai, Norimichi Noguchi, Kenji Tsubaki, and Hideki Hirayama, *Appl. Phys. Express* **10**, 031002 (2017).
- Max Shatalov *et al.*, *Appl. Phys. Express* **5**, 082101 (2012).
- Masatsugu Ichikawa, Akira Fujioka, Takao Kosugi, Shinya Endo, Harunobu Sagawa, Hiroto Tamaki, Takashi Mukai, Miyuki Uomoto, and Takehito Shimatsu, *Appl. Phys. Express* **9**, 072101 (2016).
- J. Zhang, Y. Gao, L. Zhou, Y.-U. Gil, and K.-M. Kim, "Transparent deep ultraviolet light-emitting diodes with a p-type AlN ohmic contact layer," *Proc. SPIE* **10940**, 1094002 (2019).
- Y. Matsukura, T. Inazu, C. Pernot, N. Shibata, M. Kushimoto, M. Deki, Y. Honda, and H. Amano, *Appl. Phys. Express* **14**, 084004 (2021).
- Zhang Jianping, Gao Ying, Ling Zhou, Gil Young-Un Gil, and Kyoung-Min Kim, *Semicond. Sci. Technol.* **33**, 07LT01 (2018).
- Y. Nagasawa and A. Hirano, *Appl. Sci.* **8**, 1264 (2018).
- D. Hollington, J. T. Baird, T. J. Sumner, and P. J. Wass, *Classical Quantum Gravity* **32**, 235020 (2015).
- P. J. Wass, H. M. Araújo, D. N. A. Shaul, and T. J. Sumner, *Classical Quantum Gravity* **22**, S311 (2005).
- K. X. Sun, N. Leindecker, S. Higuchi, J. Goebel, S. Buchman, and R. L. Byer, *J. Phys.: Conf. Ser.* **154**, 012028 (2009).
- S. Saraf *et al.*, *Classical Quantum Gravity* **33**, 245004 (2016).
- P. J. Wass, "LISA Pathfinder Collaboration, Free-fall performance for the LISA gravitational wave observatory: new results from LISA pathfinder," in *APS April Meeting 2018* Columbus, OH, 14–17 April 2018 (APS, 2018), Vol. 2018, p. C14.001, see <http://meetings.aps.org/link/BAPS.2018.APR.C14.1> (last accessed December 4, 2024).
- B. C. Letson, S. Barke, P. Wass, G. Mueller, F. Ren, S. J. Pearton, and J. W. Conklin, *J. Vac. Sci. Technol. A* **41**, 013202 (2023).

- <sup>22</sup>B. C. Letson, S. Barke, S. P. Kenyon, T. Olatunde, G. Mueller, P. Wass, F. Ren, S. J. Pearton, and J. W. Conklin, *Rev. Sci. Instrum.* **93**, 114503 (2022).
- <sup>23</sup>B. C. Letson, J. W. Conklin, P. Wass, S. Barke, G. Mueller, M. A. J. Rasel, A. Haque, S. J. Pearton, and F. Ren, "Reliability and Degradation Mechanisms of Deep UV AlGaIn LEDs." *ECS J. Solid State Sci. Technol.* **12**(6), 066002 (2023).
- <sup>24</sup>J. W. Conklin *et al.*, *GRATTIS: The Gravitational Reference Advanced Technology Test in Space, Small Satellites Systems and Services Symposium*, Palma de Mallorca, Spain, 27–31 May 2024 (Centre National D'etudes Spatiales, Palma de Mallorca, Spain, 2024).
- <sup>25</sup>Y. Wang *et al.*, *IEEE Trans. Nucl. Sci.* **68**, 149 (2021).
- <sup>26</sup>M. W. Moseley, A. A. Allerman, M. H. Crawford, J. J. Wierer, M. L. Smith, and A. M. Armstrong, *J. Appl. Phys.* **117**, 095301 (2015).
- <sup>27</sup>S. J. Pearton, Xinyi Xia, Fan Ren, Md Abu Jafar Rasel, Sergei Stepanoff, Nahid Al-Mamun, Aman Haque, and Douglas E. Wolfe, *J. Vac. Sci. Technol. B* **41**, 030802 (2023).
- <sup>28</sup>A. Floriduz and J. D. Devine, *Jpn. J. Appl. Phys.* **57**, 080304 (2018).
- <sup>29</sup>I. H. Lee, A. Y. Polyakov, N. B. Smirnov, I. V. Shchemerov, P. B. Lagov, R. A. Zinov'ev, E. B. Yakimov, K. D. Shcherbachev, and S. J. Pearton, *J. Appl. Phys.* **122**, 115704 (2017).
- <sup>30</sup>I. H. Lee *et al.*, *Phys. Status Solidi (a)* **214**, 1700372 (2017).
- <sup>31</sup>R. Khanna, S. Y. Han, S. J. Pearton, D. Schoenfeld, W. V. Schoenfeld, and F. Ren, "High dose Co-60 gamma irradiation of InGaIn quantum well light-emitting diodes." *Appl. Phys. Lett.* **87**(21), 212107 (2005).
- <sup>32</sup>J. C. Petrosky, J. W. McClory, T. E. Gray, and T. A. Uhlman, *IEEE Trans. Nucl. Sci.* **56**, 2905 (2009).
- <sup>33</sup>B. Luo *et al.*, *Appl. Phys. Lett.* **80**, 604 (2002).
- <sup>34</sup>S. J. Pearton, F. Ren, E. Patrick, M. E. Law, and A. Y. Polyakov, "Ionizing radiation damage effects on GaN devices." *ECS J. Solid State Sci. Technol.* **5**(2), Q35 (2015).
- <sup>35</sup>D. M. Fleetwood, *IEEE Trans. Nucl. Sci.* **60**, 1706 (2013).
- <sup>36</sup>P. Goldhagen, *MRS Bull.* **28**, 131 (2003).
- <sup>37</sup>JESD89-3B, Test Method for Beam Accelerated Soft Error Rate (2021).
- <sup>38</sup>A. Yoshikawa, R. Hasegawa, T. Morishita, K. Nagas, S. Yamada, J. Grandusky, J. Mann, A. Amy Miller, and L. J. Schowalter, *Appl. Phys. Express* **13**, 022001 (2020).
- <sup>39</sup>C. Leroy and P. G. Rancoita, *Principles of Radiation Interaction in Matter and Detection*, 4th edn. (World Scientific, Singapore, 2016), Screened Relativistic-NIEL Calculator Website, see <https://www.sr-niel.org/index.php>.
- <sup>40</sup>C. Leroy and P. G. Rancoita, *Rep. Prog. Phys.* **70**, 493 (2007).
- <sup>41</sup>J. F. Ziegler, *IBM J. Res. Dev.* **42**, 117 (1998).
- <sup>42</sup>M. Mandurrino, G. Verzellesi, M. Goano, M. Vallone, F. Bertazzi, G. Ghione, M. Meneghini, G. Meneghesso, and E. Zanoni, *Phys. Status Solidi (a)* **212**, 947 (2015).
- <sup>43</sup>D. Monti *et al.*, *IEEE Trans. Electron Devices* **64**, 200 (2017).
- <sup>44</sup>M. F. Chaiken and T. E. Blue, *IEEE Trans. Nucl. Sci.* **65**, 1147 (2018).
- <sup>45</sup>D. B. Pelowitz, "MCNPX user's manual: Version 2.7.0," Technical Report No. LA-CP-11-00438, Los Alamos National Laboratory, Los Alamos, NM, 2011.
- <sup>46</sup>Nicola Rocco *et al.*, *Appl. Phys. Lett.* **122**, 161105 (2023).
- <sup>47</sup>N. Rocco *et al.*, *IEEE Photonics J.* **16**, 8200206 (2024).
- <sup>48</sup>Z. Ma, H. Cao, S. Lin, X. Li, and L. Zhao, *Solid-State Electron.* **156**, 92 (2019).
- <sup>49</sup>F. Piva *et al.*, *Photonics Res.* **8**, 1786 (2020).
- <sup>50</sup>H. Masui, *Semicond. Sci. Technol.* **26**, 075011 (2011).
- <sup>51</sup>J. M. Shah, Y. L. Li, T. Gessmann, and E. F. Schubert, *J. Appl. Phys.* **94**, 2627 (2003).
- <sup>52</sup>G. P. Summers, E. A. Burke, P. Shapiro, S. R. Messenger, and R. J. Walters, *IEEE Trans. Nucl. Sci.* **40**, 1372 (1993).
- <sup>53</sup>Total dose steady-state irradiation test method, European space components, coordination basic specification No. 22900, see <http://escies.org/escs-specs/publishe/d/22900.pdf> (2016).
- <sup>54</sup>S. O. Kucheyev, J. S. Williams, J. Zou, C. Jagadish, M. Pophristic, S. Guo, I. T. Ferguson, and M. O. Manasreh, *J. Appl. Phys.* **92**, 3554 (2002).